Optical Materials 54 (2016) 57–66

Contents lists available at ScienceDirect

Optical Materials

journal homepage: www.elsevier.com/locate/optmat

Luminescence properties of Yb:Er:KY_3F_{10} nanophosphor and thermal treatment effects

Laércio Gomes [a,*], Horácio Marconi da Silva M.D. Linhares [b], Rodrigo Uchida Ichikawa [c], Luis Gallego Martinez [c], Sonia Licia Baldochi [a]

[a] Centro de Lasers e Aplicações, Instituto de Pesquisas Energéticas e Nucleares, IPEN-CNEN/SP, Butantã, P.O. Box 11049, São Paulo, SP 05422-970, Brazil
[b] Instituto do Noroeste Fluminense de Educação Superior, Universidade Federal Fluminense, UFF, Santo Antonio de Padua, P.O. Box 121799, Rio de Janeiro, RJ 28470, Brazil
[c] Departamento de Ciências dos Materiais, Instituto de Pesquisas Energéticas e Nucleares, IPEN-CNEN/SP, Butantã, P.O. Box 11049, São Paulo, SP 05422-970, Brazil

ARTICLE INFO

Article history:
Received 18 December 2015
Received in revised form 19 January 2016
Accepted 8 February 2016

Keywords:
Time-resolved luminescence spectroscopy
Rare-earth luminescence
Energy transfer rate parameters
Upconversion luminescence
Luminescence efficiency
Nanophosphors

ABSTRACT

In this work, we present the spectroscopic properties of KY_3F_{10} nanocrystals activated with erbium and codoped with ytterbium ions. The most important processes that lead to the erbium upconversion of green and red emissions of Er^{3+} were identified. A time-resolved luminescence spectroscopy technique was employed to measure the luminescence decays of $^4S_{3/2}$ and $^4F_{9/2}$ excited levels of Er^{3+} and to determine the upconversion processes and the luminescence efficiencies of erbium in the visible. Analysis of the luminescence kinetics in Yb:Er:KY_3F_{10} shows a rapid upconversion (Up_1) for the green emission with a time constant of 0.31 μs after pulsed laser excitation at 972 nm for as synthesized nanocrystals, which is faster than the time constant measured for the bulk crystal (23 μs). In addition, it is observed a second upconversion process (non-resonant) (Up_2) responsible for the red emission (Er^{3+}), which competes with Up_1 process. However, the luminescence efficiency of the green emission ($^4S_{3/2}$) is observed to be very low (1.6%) for the as synthesized nanocrystal (25 °C). Nevertheless, it increases with the nanopowder heat treatment reaching an efficiency of 99% (T = 550 °C) relative to the bulk crystal. Similar luminescence behavior was observed for the $^4F_{9/2}$ level (Er^{3+}) that emits red emission. X-ray diffraction analysis of nanopowder by Rietveld method reveled that the mean crystallite size remains unchanged (8.3–12.3 nm) after thermal treatments with T ~ 400 °C, while the $^4S_{3/2}$ luminescence efficiency strongly increases to 20%. The luminescence dynamics indicates that Er^{3+} ions distribution plays a determinant role in the luminescence efficiency of green and red emissions of Er^{3+} besides also the strong influence on the upconversions processes. The observed luminescence effect is caused by the non-uniform Er^{3+} (and Yb^{3+}) ions distribution due to the nanocrystal grown, which introduces a concentration gradient that increases towards the nanoparticle surface. This concentration effect produces strong (Er × Er) cross-relaxations depleting the excited states populations of $^4S_{3/2}$ and $^4F_{9/2}$ levels and their luminescence efficiencies in KY_3F_{10} nanocrystals. The concentration gradient is very accentuated in the as synthesized nanocrystal and gradually decreases with the thermal treatments where the dopant ions can migrate through the lattice towards the nanocrystal's interior to get a more uniform and random distribution, which is reached after heat treatment to T = 550 °C.

1. Introduction

With the oncoming of the nanoscience and nanotechnology in the past few decades, this new field has exerted great impact on upconversion materials, then studies on the synthesis and properties of upconversion nanophosphors [1] have received intense research interest due to their application as luminescent labels in bioimaging, and as donors in energy transfer systems [2,3]. These nanomaterials, capable of converting near infrared (NIR) photons to higher energy photons ranging from ultraviolet (UV) to NIR, allow the excitation to fall in the so-called "optical window" (~650–1300 nm), i.e. the optimal spectral range for minimal absorption by human tissue and negligible auto-fluorescence of the biological background. They are thus expected to be able to significantly improve the quality of the luminescence biomedical imaging, labeling and therapy.

Despite this progress, the satisfactory upconversion efficiency remains one of the main obstacles on the way to actual application. The upconversion efficiency is only several percent in a macroscopic

* Corresponding author.
E-mail address: lgomes@ipen.br (L. Gomes).

http://dx.doi.org/10.1016/j.optmat.2016.02.010
0925-3467/

crystal under 980 nm excitation, and the highest upconversion efficiency in nano-size materials so far is more than one order of magnitude lower under the same excitation conditions. For example, under 980 nm continuous excitation (CW) of 150 W cm^{-2} the highest upconversion quantum yield is reported around 0.1% for Yb^{3+}/Er^{3+} co-doped $NaYF_4$ core-shell nanoparticles of 30 nm in diameter [4]. This situation has triggered the following question raised in Ref. [5]: what are the responsible channels/steps for the loss of the excitation energy in the nanomaterials?

In order to obtain answers to this question, a comprehensive study of the upconversion luminescence in Yb^{3+}/Er^{3+} co-doped and Er^{3+} doped KY_3F_{10} nanocrystals have been done in order to investigated the luminescence kinetics of the main excited states of Er^{3+}, $^4S_{3/2}$, $^4F_{9/2}$, which exhibit green and red emissions under 972 nm laser excitation. A time-resolved luminescence spectroscopy under selective pulsed laser excitations was employed as an important technique to investigate the nature of these processes and the luminescence efficiencies.

KY_3F_{10} crystal is a suitable host for trivalent rare-earth ions like Yb^{3+}, Tm^{3+}, Er^{3+} or Ho^{3+} ions, which can easily substitute Y^{3+} ions in a non-center-symmetrical site [C_{4v} symmetry] [6,7–10]. KY_3F_{10} is the only compound in the KF-YF_3 system that melts congruently without any phase transition. It crystallizes in the cubic fluorite-type structure ($Fm3m$) with a lattice parameter a = 11.553 Å [10], which constitutes an isotropic crystal. In particular, Yb(20%):Er(0.5%):KY_3F_{10} can be synthesized as nanocrystals able to efficiently emit at 542 nm (and 667 nm) when excited at 972 nm due to its relatively low phonon energy (cut off $\sim$ 500 cm^{-1}) that is an important point in avoiding energy loss by non-radiative relaxation involving the $^4S_{3/2}$ excited level of Er^{3+} [11–13].

In this paper, nanocrystals of Yb:Er:KY_3F_{10} sizing 8.3 nm were synthesized by co-precipitation method in aqueous solution. The multiple processes of energy transfer that occurs when this material is excited around 972 nm were inspected and the transfer time constants were determined. The upconversion luminescence transients at 542 nm and 667 nm, respectively from the $^4S_{3/2}$ and $^4F_{9/2}$ excited states of Er^{3+} were measured for Yb(20 mol.%):Er(0.5 mol.%):KY_3F_{10} nanocrystals excited by pulsed laser excitation at 972 nm. The luminescence efficiencies of $^4S_{3/2}$ and $^4F_{9/2}$ excited states were measured and the dependence on the thermal treatment temperature and crystallite size were determined.

2. Experimental procedure

The nanopowders were obtained by the co-precipitation method [14–16], boiling aqueous solution of potassium fluoride (KF – Merck, 99%) was slowly added in a hot $RECl_3$ aqueous solution (RE = Y, Yb, Er), followed by slow addition of an ammonium bifluoride boiling aqueous solution (NH_4HF_2 – Aldrich, 98%). Rare earth fluorides were obtained from ReO_3 (Aldrich, 99.9%) dissolved in concentrated hydrochloric acid. After the addition of the NH_4HF_2 solution a white precipitate was formed, and the resulted solution was maintained at 80 °C and stirring for 3 h. The initial molar proportion was of 1 KF + $(1-x)$ YCl_3 + x $LnCl_3$ + 3 NH_4HF_2, where Ln = Yb and Er. The nanocrystals were separated by centrifugation and the fine powder was collected, washed with Milli-Q water several times and dried in air in a hot plate at 40 °C for 48 h. Thermal treatments at different temperatures were carried out at a resistive oven for 6 h under argon flow (White Martins, 99.995%), using an amount of the synthesized nanopowder and extracting aliquots of it at every interest temperature, to perform the spectroscopic studies. In addition, we performed the luminescence measurements using a water solution with dispersed nanocrystals before and after hydrothermal treatments to T = 200 °C for different treatment times of 24, 36, 48 and 60 h for comparison and discussion.

Samples (nanopowders) were characterized by X-ray diffraction (XRD) on a Panalytical ŔPERT diffractometer and by transmission electronic microscopy (TEM) on a JEOL JEM 200C microscope with accelerating voltage of 200 kV. Lattice parameters were obtained by Rietveld refinement method using a GSAS-EXPGUI program [17,18] and the mean crystallite diameters (d) using Rietveld or the single line methods [19]. The mean crystallite size was estimated through Rietveld refinement using the software TOPAS 4.2 [20] applying a macro that convolutes Gaussians and Lorenztians related to the size broadening in the X-ray diffraction (XRD) profile. Also, the instrumental contribution needs to be corrected to provide reliable results. For this, a highly crystalline sample of Y_2O_3 was measured, refined and taken into account in the Yb:Er:KY_3F_{10} refinements. The modified Thompson-Cox-Hastings function (TCHZ) was used to fit the profile. The mean crystallite size here determined is the so-called volume weighted mean crystallite size as defined by Balzar et al. [21].

The absorption spectra of all samples were measured in the range 400–1200 nm at room temperature using a Varian Cary 5000 spectrophotometer working in the diffuse reflection mode, where an integrating sphere was used. In the luminescence lifetime measurements, the samples were excited by pulsed laser radiation generated by a tunable OPO-IR pumped (Rainbow from OPOTEK, USA) by the second harmonic of a Q-switched Nd:YAG (yttrium aluminum garnet) laser (Brilliant B from Quantel, France). Laser pulse widths of 10 ns at 972 nm were used to directly excite the $^4F_{5/2}$ excited state of Yb^{3+}. Luminescence signals were analyzed by the 0.25 m Kratos monochromator, detected by the EMI S-20 (or S-1) PMT (response time of 10 ns) or InSb 77 K infrared detector from Judson (response time $\sim$ 0.5 μs) or using a charge coupled device (CCD) spectrometer coupled to the sample holder containing the nanopowder via optical fiber. Luminescence lifetime was measured using a digital oscilloscope of 100 MS s^{-1} model TDS 410 from TEKTRONIX interfaced to a microcomputer.

3. Experimental results

The synthesized nanopowders have shown the cubic phase ($Fm\bar{3}m$) of KY_3F_{10} corresponding to the fluorite crystalline structure, however with the diffraction peaks wider due to the small size of nanocrystals and defects as seen in Fig. 1. Nevertheless, X-ray diffraction peaks become narrow after thermal treatment at T = 550 °C due to the particles growth and increasing of crystallinity (Fig. 1). The synthesized nanocrystals were approximately

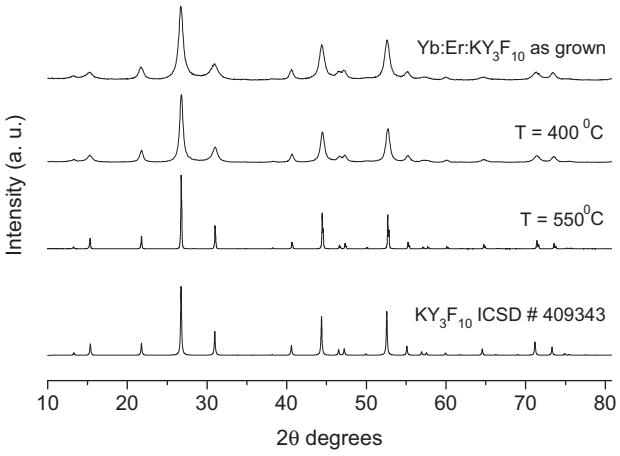

Fig. 1. X-ray diffraction pattern of Yb(20%):Er(0.5%):KY_3F_{10} synthesized nanopowder before (as grown) and after thermal treatments at T = 400 °C and 550 °C. A diffraction pattern obtained for a KY_3F_{10} bulk crystal was included for comparison.

spherical with a mean diameter of 8.3 nm as shown by TEM photograph (Fig. 2). Despite the small mean crystal size obtained after synthesis, Yb:Er:KY_3F_{10} has well-defined crystalline phase as can be seen in the transmission micrograph shown in Fig. 3.

Rietveld refinement of the XRD patterns considering the cubic structure with space group $Fm\bar{3}m$ (ICSD 409643) and spherical particles yielded lattice parameter of 11.499 Å for KY_3F_{10} nanocrystals and the mean crystallite size d (nm) before and after the Yb:Er:KY_3F_{10} nanopowder thermal treatments. The smaller cell parameter for the Yb/Er doped nanocrystal compared to the bulk crystal (11.553 Å) is due to the codoping with Yb^{3+} ions, which have smaller ionic radii than the yttrium one. After thermal treatments, the XRD peaks were narrowed due to particles growth and the increasing of crystallinity (Fig. 1). TEM analysis confirmed the result obtained for the synthesized particles sizes. The changes in the mean crystallite sizes (d) after heating of the samples at diverse temperatures are given in the following: d = 8.3 nm (as grown, 25 °C); d = 8.1 nm (T = 140 °C); d = 8.1 nm (200 °C); d = 9.5 nm (300 °C); d = 12.3 nm (400 °C); d = 31.5 nm (450 °C); d = 53 nm (500 °C) and d = 85 nm (550 °C).

Optical absorption spectrum of Yb:Er doped KY_3F_{10} bulk crystal has two main absorptions in the near infrared centered at 960 nm (Yb^{3+}) and 975 nm due to Er^{3+} ions. The $^4I_{15/2} \rightarrow {}^2H_{11/2}$ absorption transition of Er^{3+} in Yb:Er:KY_3F_{10} synthesized nanocrystals (as grown) is shown in Fig. 4. The small absorption peak at 523 nm that is lacking for the synthesized (as grown) nanopowder appears after the thermal treatment to T = 450 °C and it becomes more evident after T = 550 °C, where the absorption structure tends to fit the bulk crystal absorption. This indicates that crystallinity of the nanoparticle improves with the thermal treatment at T > 450 °C, as is shown also by the X-ray diffraction pattern (Fig. 1). Fig. 4 also shows that the absorption intensity (integrated) of both $^4I_{15/2} \rightarrow {}^2H_{11/2}$ and $^4I_{15/2} \rightarrow {}^4S_{3/2}$ transitions measured for Yb:Er:KY_3F_{10} synthesized (as grown) nanopowder decreases with the thermal treatment. It was measured an absorption decrease by a factor of 5.6 after the thermal treatment at T = 450 °C compared to the absorption intensity (integrated) of the synthesized (as grown) nanopowder. Because the crystallite diameter remains approximately constant (8.3 nm → 31.5 nm) under thermal treatments with temperatures below 500 °C, we can infer that the absorption decrease observed in Fig. 4 is related to the Er^{3+} ion diffusion through the interior of the nanoparticle induced by the thermal treatment (concentration effect). As the thermal treatment temperature increases the Er^{3+} ion migrates through the nanocrystal lattice to minimize structure tensions, while getting a more uniform concentration or random ions distribution. In this case, the absorption intensity taken from the diffuse reflectivity measurement, which contains large contribution from the nanoparticle surface, decreases. However, the thermal treatment at T = 550 °C promotes the nanoparticle growth and consequently the absorption increases a little as seen in Fig. 4. The dependence of the scattering intensity on the wavelength (λ) light was measured near the Er^{3+} absorptions in the visible region, which showed the usual intensity dependence over $1/\lambda^n$ with $4 > n > 2$. However this scattering intensity decreases monotonically with the wavelength and do not introduce any modification in the Er^{3+} absorption bands

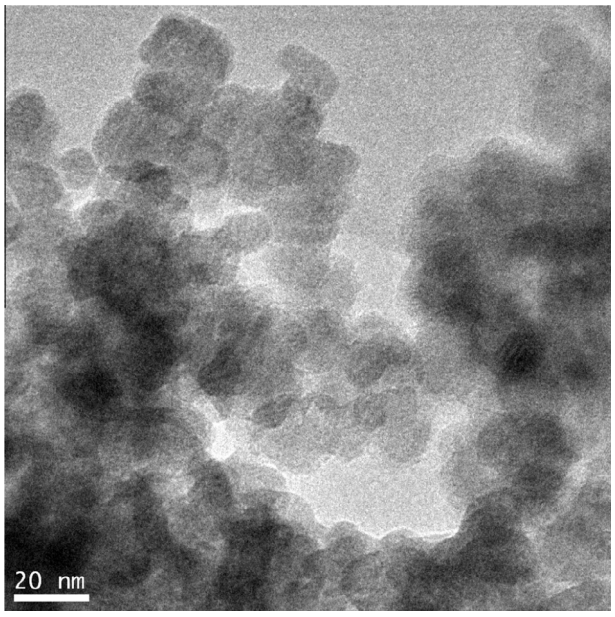

Fig. 2. TEM micrograph obtained for nanopowder Yb(20%):Er(0.5%):KY_3F_{10} synthesized (as grown).

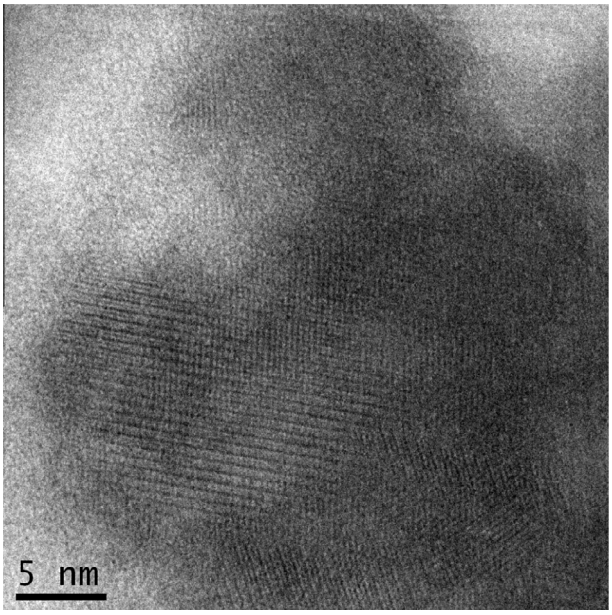

Fig. 3. TEM micrograph obtained for nanopowder Yb(20%):Er(0.5%):KY_3F_{10} synthesized (as grown) with an improved resolution. HRTEM image provides the lattice planes of cubic KY_3F_{10} struture.

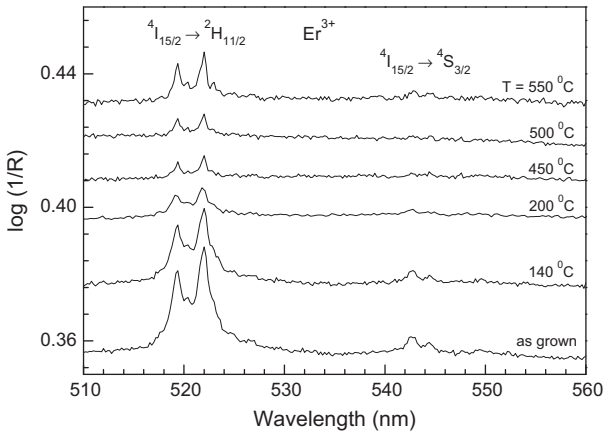

Fig. 4. The $^4I_{15/2} \rightarrow {}^2H_{11/2}$ and $^4I_{15/2} \rightarrow {}^4S_{3/2}$ absorption transitions of Er^{3+} in Yb (20%):Er(0.5%):KY_3F_{10} synthesized nanocrystals (as grown) and for the thermally treated samples at T = 140, 200, 450, 500 and 550 °C are shown. Absorption intensity, log (1/R) was calculated using the measure data of diffuse reflectance (R) of nanopowder.

structure once the nanopowder is constituted by particles that have a mean size much smaller than the wavelength light.

When Yb:Er:KY_3F_{10} bulk crystal is excited at 972 nm, green (530–560) nm Er^{3+} emission is observed and the upconversion intensity (green emission) strongly increases for ytterbium concentration higher than 10 mol.% [22]. Best ytterbium concentration, which maximizes the blue upconversion luminescence of Tm^{3+} ($^1G_4$) is ~20 mol.% for Yb:Nd:Tm doped KY_3F_{10} crystal, where ytterbium and neodymium ions are used as sensitizers [22]. This luminescence effect indicates that Yb^{3+} ions significantly contribute to the population of the $^4S_{3/2}$ excited level that emits around 542 nm.

Fig. 5 shows the schematic energy diagram levels of Yb:Er proposed for Er^{3+} ($^4S_{3/2}$ and $^4F_{9/2}$) upconversions (Up_1 and Up_2), which will be discussed and proved to be essential for the green and red emissions of nanocrystals taking into account the luminescence dynamics analysis in sequence. When the Yb:Er samples are excited at (972) nm the following processes are observed to compete (Up_1 and Up_2) to excite the green and red emissions from Er^{3+}:

(1) ET_1: Yb^{3+} ($^4F_{5/2}$) + Er^{3+} ($^4I_{15/2}$) → Yb^{3+} ($^4F_{7/2}$) + Er^{3+} ($^4I_{11/2}$) (resonant process)
(2) ET_2: Yb^{3+} ($^4F_{5/2}$) + Er^{3+} ($^4I_{15/2}$) → Yb^{3+} ($^4F_{7/2}$) + Er^{3+} ($^4I_{13/2}$) (non-resonant process)
(3) Up_1: Yb^{3+} ($^4F_{5/2}$) + Er^{3+} ($^4I_{11/2}$) → Yb^{3+} ($^4F_{7/2}$) + Er^{3+} ($^4F_{7/2}$) → Er^{3+} ($^4S_{3/2}$)
(4) Up_2: Yb^{3+} ($^4F_{5/2}$) + Er^{3+} ($^4I_{13/2}$) → Yb^{3+} ($^4F_{7/2}$) + Er^{3+} ($^4F_{9/2}$)
(5) CR_1: Er^{3+} ($^4S_{3/2}$) × Er^{3+} ($^4I_{15/2}$) → Er^{3+} ($^4I_{11/2}$) + Er^{3+} ($^4I_{13/2}$)
(6) CR_2: Er^{3+} ($^4F_{9/2}$) × Er^{3+} ($^4I_{15/2}$) → Er^{3+} ($^4I_{13/2}$) + Er^{3+} ($^4I_{13/2}$)

ET is used to represents the non-radiative energy transfer; Up for the upconversion process and CR is representing the cross-relaxation process. The upconversion process Up_2 is observed to compete with the Up_1 process and is first proposed in this work.

The spectrum of upconversion emission of Er^{3+} involving the $^4S_{3/2} \rightarrow {}^4I_{15/2}$ (542 nm) and $^4F_{9/2} \rightarrow {}^4I_{15/2}$ (667 nm) transitions is shown in Fig. 6 for the synthesized nanopowder (as grown) and for the thermally treated (TT) ones at T = 140, 200, 300, 450 and 550 °C, where the luminescence was excited by pulsed laser at 972 nm using an excitation intensity of 2×10^6 W cm^{-2} (E = 5 mJ). The result exhibited in Fig. 6 shows that both green and red emissions have similar integrated intensities such as the ratio of the green emission to red (RGR) is equal to 0.786 for the as grown nanopowder (25 °C). However, it is seen that both

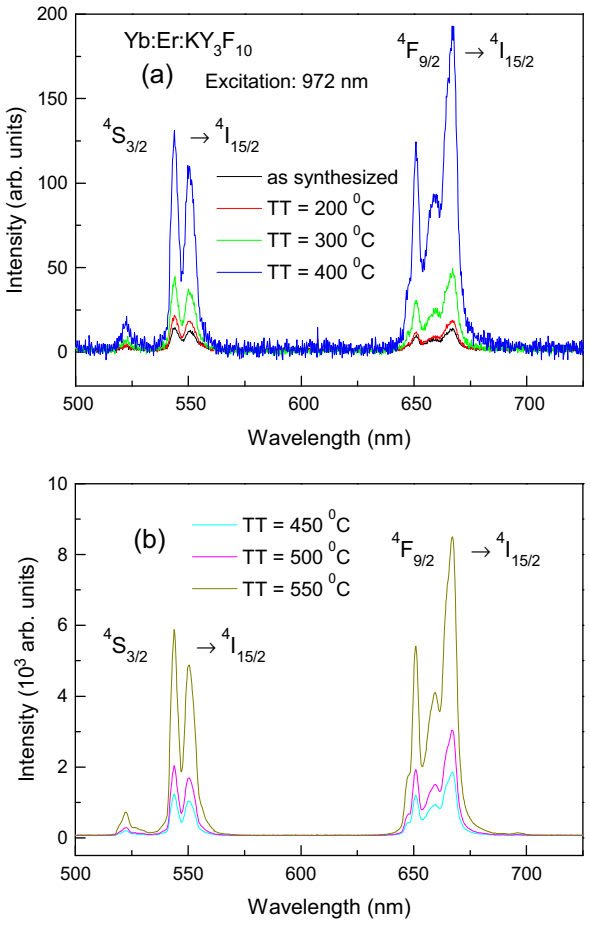

Fig. 6. Upconversion emission spectrum of Er^{3+} in Yb(20%):Er(0.5%):KY_3F_{10} synthesized nanopowder (as grown) and after thermal treatments at T = 200, 300, 400, 450, 500 and 550 °C. The luminescence transient was excited using pulse laser excitation at 972 nm with an intensity of 2×10^6 W cm^{-2} per pulse (E = 5 mJ).

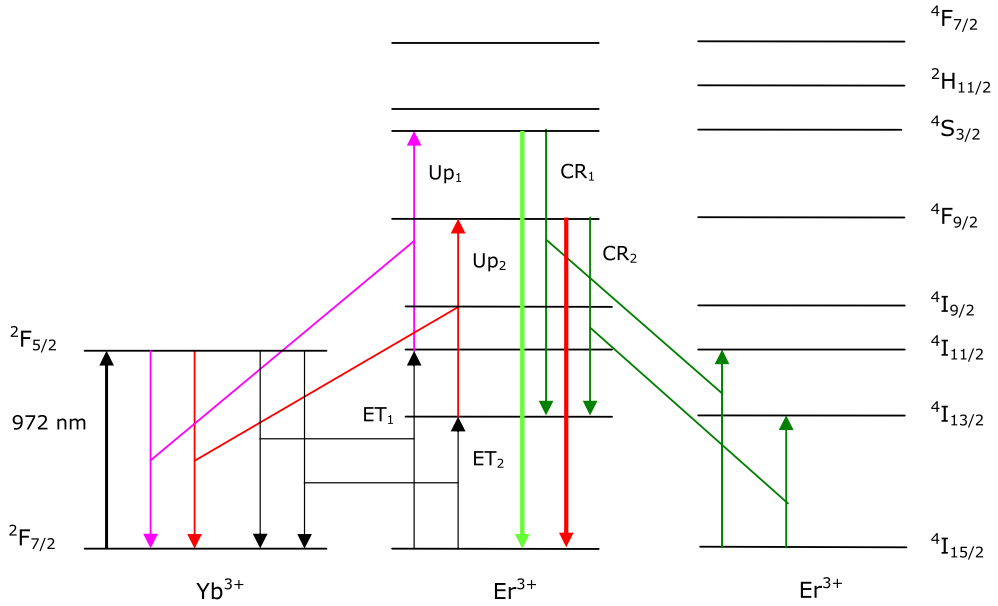

Fig. 5. Energy levels diagram proposed for Yb:Er:KY_3F_{10} nanocrystal. ET was used for representing the non-radiative energy transfer, CR was used for cross-relaxation and Up_1 and Up_2 were used for the upconversion processes.

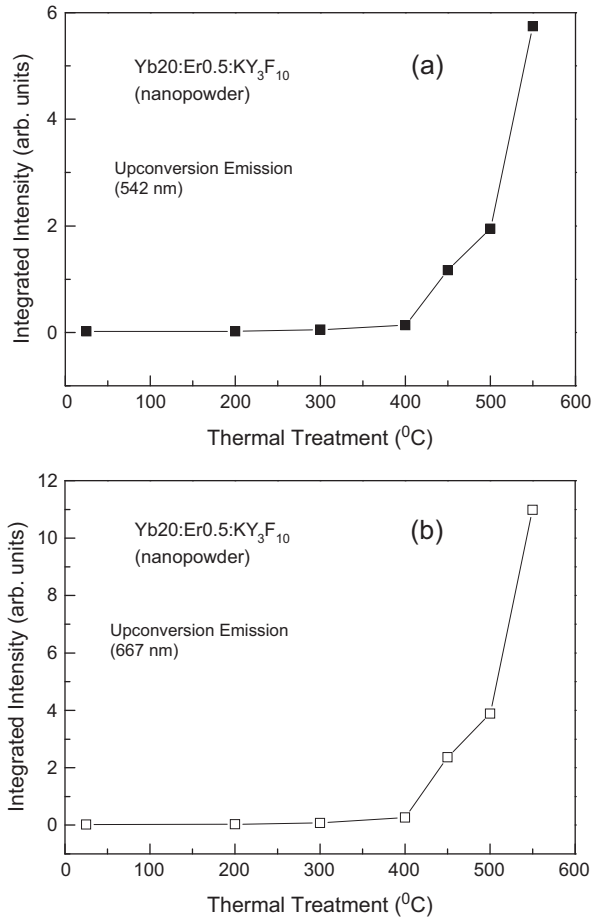

Fig. 7. Upconversion luminescence integrated intensity for green emission (a) (from 500 to 570 nm) and red emission (b) (from 620 to 700 nm) of Er^{3+} in Yb(20%):Er(0.5%):KY_3F_{10} synthesized nanopowder (as synthesized) and for the thermally treated ones with treatments temperatures at T = 200, 300, 400, 450, 500 and 550 °C. A pulse laser excitation intensity of 2×10^6 W cm^{-2} at 972 nm per pulse was used (E = 5 mJ).

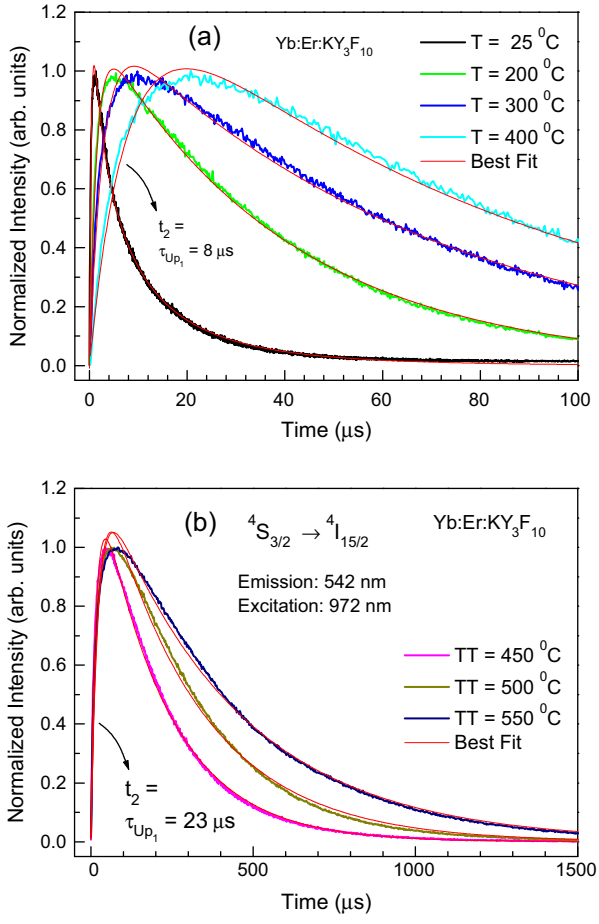

Fig. 8. Upconversion luminescence transient of $^4S_{3/2}$ level of Er^{3+} measured at 542 nm for synthesized nanopowder (as synthesized, T = 25 °C) and for the thermally treated ones at temperatures (a) T = 200, 300, 400 °C and (b) T = 450, 500 and 550 °C. A laser excitation intensity of 2×10^6 W cm^{-2} at 972 nm was used (E = 5 mJ). The emission intensities were normalized to one in order to visually compare the strong differences between the curves.

emissions intensities strongly increases with the thermal treatment above 400 °C. The RGR value decrease to 0.523 after the thermal treatment at T = 550 °C (see Fig. 7).

The luminescence kinetic of an acceptor state that is indirectly excited by the donor-acceptor (or D-A) energy transfer is given by Eq. (1), which has been derived elsewhere [23] for an energy transfer that includes Burshtein (or Inokuti-Hirayama, where ω = 0) model for the donor decay due to a dipole-dipole interaction [24].

$$I(t) = I_0\left\{exp\left(-\frac{t}{\tau_a}\right) - exp\left(-\frac{t}{\tau_d} - \omega t - \gamma\sqrt{t}\right)\right\}, \quad (1)$$

where τ_a is the luminescence lifetime of the acceptor (A) excited state and τ_d is the intrinsic lifetime of the donor (D) excited ion. γ is the energy transfer parameter (given in $s^{-1/2}$) due to the donor to acceptor direct transfer and ω is the energy transfer parameter (given in s^{-1}) due to the migration contribution through donor excited level. The first term of Eq. (1) gives the luminescence decay of the acceptor and the second gives the luminescence risetime, which should be equal to the donor total lifetime. The risetime constant was obtained by integration according to Eq. (2) for the case of a non-exponential process.

$$\tau = \int_0^\infty exp\left(-\frac{t}{\tau_d} - \omega t - \gamma\sqrt{t}\right)dt. \quad (2)$$

For instance, if the diffusion process between donor states dominates the energy transfer mechanism (or $\omega \gg \gamma^2$) the donor decay will be exponential and the acceptor risetime will be exponential. That is the case observed of Yb^{3+} ($^2F_{5/2}$) → Er^{3+} ($^4I_{11/2}$) transfer (Up_1) in Yb:Er system observed in this work because it involves a resonant transfer besides the high Yb^{3+} concentration used (20 mol.%). In this case, the acceptor luminescence fitting was performed using Eq. (3) that has been used to describe the upconversion kinetic [12,23–28].

$$I(t) = A\left\{exp\left(-\gamma\sqrt{t} - \frac{t}{t_1}\right) - exp\left(-\frac{t}{t_2}\right)\right\}. \quad (3)$$

The fitting parameters t_1 and γ are used to describe the decay time of $^4S_{3/2}$ (Er^{3+}) excited state due to a strong cross-relaxation (CR_1) effect observed in Yb:Er:KY_3F_{10} nanocrystals and t_2 gives the characteristic time of the upconversion (Up_1) process (risetime of green emission). On the other hand, the fitting of 667 nm emission transient showed that the upconversion process appears as a decay of the red emission and parameters t_1 and γ are used to describe the upconversion process Up_2. In this case, t_2 gives the decay time constant of the $^4F_{9/2}$ excited state that includes a cross-relaxation (CR_2) process and should appears as the rise time of red emission, i.e., t_2 is much shorter than the upconversion time (Up_2).

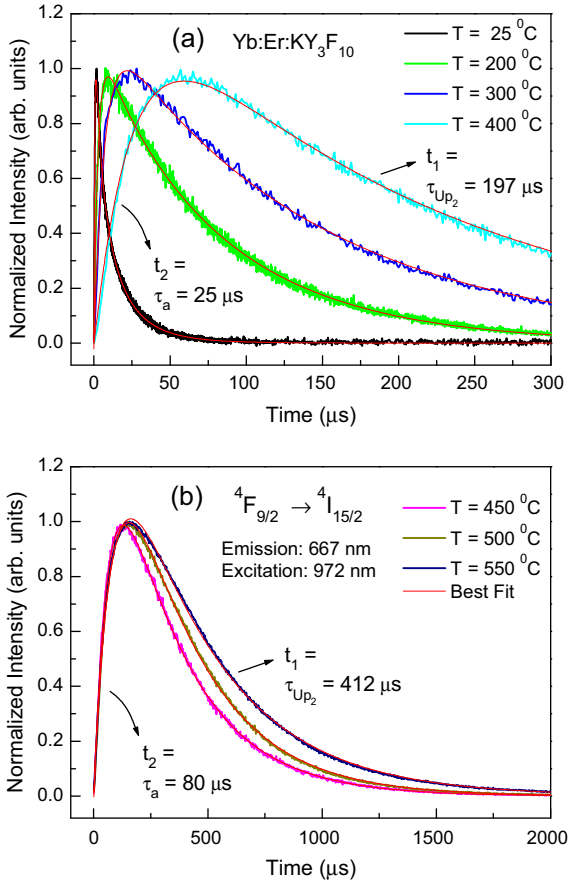

Fig. 9. Upconversion luminescence transient of $^4F_{9/2}$ level of Er^{3+} measured at 667 nm for synthesized nanopowder (as synthesized, T = 25 °C) and for the thermally treated ones at temperatures (a) T = 200, 300, 400 °C and (b) T = 450, 500 and 550 °C. A laser excitation intensity of 2×10^6 W cm^{-2} at 972 nm was used (E = 5 mJ). The emission intensities were normalized to one in order to visually compare the strong differences between the curves.

The upconversion luminescence kinetic of green (at 542 nm) and red (at 667 nm) due to the $^4S_{3/2}$ and $^4F_{9/2}$ levels emissions of Er^{3+} were excited by laser pulse at 972 nm for Yb:Er:KY_3F_{10} as grown and thermally treated nanopowders at several temperatures. The luminescence transients for green emission are seen in Fig. 8. Fig. 9 shows the luminescence transients measured for the red emission. Best fit of 542 nm and 667 nm emissions were performed using $I(t)$ expression given by Eq. (3) from where best fitting parameters γ, t_1, t_2 are the derived parameters using a least squares fit with a correlation coefficient R^2. The best fitting parameters obtained for both luminescence transients, green and red emissions are given in Tables 1 and 2, respectively. Table 3 shows the measured decay time constants (lifetime) of the main luminescence levels of Er^{3+} (0.5 mol.%) in KY_3F_{10} bulk crystals.

The results presented in Tables 1 and 2 show that t_{Up1} is always shorter then t_{Up2} and that t_{Up2} strongly depends on the thermal treatment temperature, i.e., t_{Up2} = 8.2 μs (25 °C) and t_{Up2} = 412 μs at T = 550 °C. The decay time constant measured for the thermally treated nanopowder at T = 550 °C tends to fit the luminescence decay found for the Er(0.5%):KY_3F_{10} bulk crystal, which has a lifetime τ = 418 μs for $^4S_{3/2}$ (green emission) and τ = 115 μs for $^4F_{9/2}$ (red emission) levels decay. Using the experimental lifetimes of $^4S_{3/2}$ and $^4F_{9/2}$ levels (t_1 and t_2) given in Tables 1 and 2 it were constructed Figs. 10 and 11, where Fig. 10 shows the dependence of the time constants (t_1 and t_2) of $^4S_{3/2}$ level on the temperature of thermally treated nanopowders. Fig. 11 was constructed to show

Table 1
Experimental values of the $^4S_{3/2}$ excited state decay parameters t_1 and γ ($s^{-1/2}$) and the upconversion (Up_1) time constant (t_2) obtained from best fitting of experimental luminescence kinetic curves using Eq. (3) obtained for Yb(20%):Er(0.5%):KY_3F_{10} after thermal treatments at many temperatures.

Thermal treatment	γ ($s^{-1/2}$)	t_1 (decay of $^4S_{3/2}$) (τ_1) (integrated)	t_2 (Up_1)	R^2
25 °C	489	73.5 ± 0.2 μs (τ_1 = 6.7 μs)	0.31 ± 0.02 μs	0.997
140 °C	100	12.4 ± 0.1 μs (τ_1 = 9.2 μs)	0.84 ± 0.02 μs	0.996
200 °C	25	40.0 ± 0.2 μs (τ_1 = 35 μs)	1.65 ± 0.02 μs	0.998
300 °C	0	66.9 ± 0.6 μs	2.74 ± 0.02 μs	0.998
400 °C	0	81.8 ± 0.8 μs	7.56 ± 0.02 μs	0.998
450 °C	0	209.1 ± 2 μs	16.4 ± 0.2 μs	0.999
500 °C	0	294.3 ± 3 μs	22.8 ± 0.2 μs	0.997
550 °C	0	413 ± 4 μs	22.6 ± 0.2 μs	0.998

Table 2
Experimental values of the lifetime of $^4F_{9/2}$ excited state (t_2) and the upconversion (Up_2) parameters t_1 and γ ($s^{-1/2}$) obtained from best fitting of experimental luminescence kinetic curves using Eq. (3) obtained for Yb(20%):Er(0.5%):KY_3F_{10} after thermal treatments at many temperatures.

Thermal treatment	γ ($s^{-1/2}$)	t_1 (Up_2) (τ_1) (integrated)	t_2 (decay of $^4F_{9/2}$)	R^2
25 °C	389.6 ± 3.5	47.2 ± 0.9 μs (8.2 μs)	0.48 ± 0.02 μs	0.997
140 °C	125.5 ± 16.5	13.1 ± 0.4 μs (8.9 μs)	0.84 ± 0.01 μs	0.995
200 °C	25 ± 1	92.5 ± 0.1 μs (75 μs)	2.74 ± 0.02 μs	0.998
300 °C	9.9 ± 0.5	151.7 ± 0.2 μs (136 μs)	6.99 ± 0.02 μs	0.999
400 °C	8.0 ± 0.3	218.6 ± 0.2 μs (197 μs)	24.5 ± 0.1 μs	0.999
450 °C	7.7 ± 0.3	312.8 ± 0.4 μs (278 μs)	66.9 ± 0.6 μs	0.999
500 °C	1.35 ± 0.05	324.6 ± 0.2 μs (318 μs)	85.1 ± 0.3 μs	0.999
550 °C	0	411.6 ± 0.1 μs (412 μs)	85.0 ± 0.2 μs	0.999

Table 3
Experimental values of the lifetimes of the main luminescence levels of Er^{3+} in Er (0.5 mol.%) doped KY_3F_{10} crystal (bulk). Tunable pulsed laser excitation of 10 ns (10 Hz) with E ~ 5 mJ was employed to directly excite a probe level. Lifetimes (τ) were obtained from best fitting of experimental luminescence decay using an exponential decay.

Excited level (Er^{3+})	Radiative Lifetime (τ_R)[a]	Lifetime (Expt.) (τ)[b] (non-radiative process)	Luminescence Efficiency (%)
$^4S_{3/2}$ (exc. 545 nm) (emis. 550 nm)	590 μs	418 μs ([Er] = 0.5%) (cross-relaxation)	71
$^4F_{9/2}$ (exc. 646 nm) (emis. 667 nm)	1.1 ms	115 μs (multiphonon decay)	11
$^4I_{11/2}$ (exc. 975 nm) (emis. 2750 nm)	5.5 ms	4.5 ms	100
$^4I_{13/2}$ (exc. 1490 nm) (emis. 1560 nm)	6.5 ms	14.4 ms	100

[a] Values obtained from Ref. [32].
[b] Lifetimes measured in this work.

also the time constants dependence on the temperature of thermally treated nanopowders obtained from the luminescence transient analysis of the $^4F_{9/2}$ excited level. Figs. 10(a) and 11(a) show that the lifetimes of both $^4S_{3/2}$ and $^4F_{9/2}$ levels are very short for the synthesized nanopowder (as grown), which are 6.68 μs for $^4S_{3/2}$

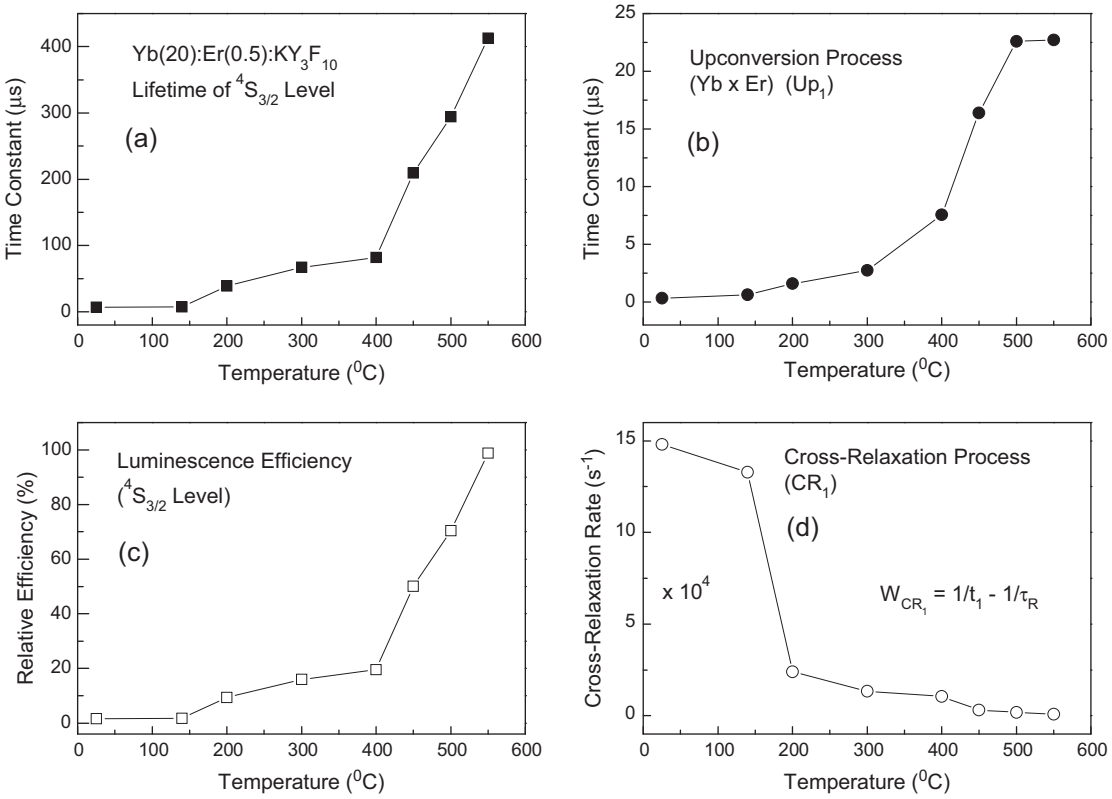

Fig. 10. Plot of measured lifetime of $^4S_{3/2}$ level of Er^{3+} (a), time constant of Yb^{3+} ($^2F_{5/2}$) × Er^{3+} ($^4I_{11/2}$) Up_1 process (b), luminescence efficiency ($^4S_{3/2}$) (c), and cross-relaxation rate (s^{-1}) calculated for $^4S_{3/2}$ level of Er^{3+} (d) as a function of the thermal treatment temperatures for Yb(20%):Er(0.5%):KY_3F_{10} synthesized nanopowder.

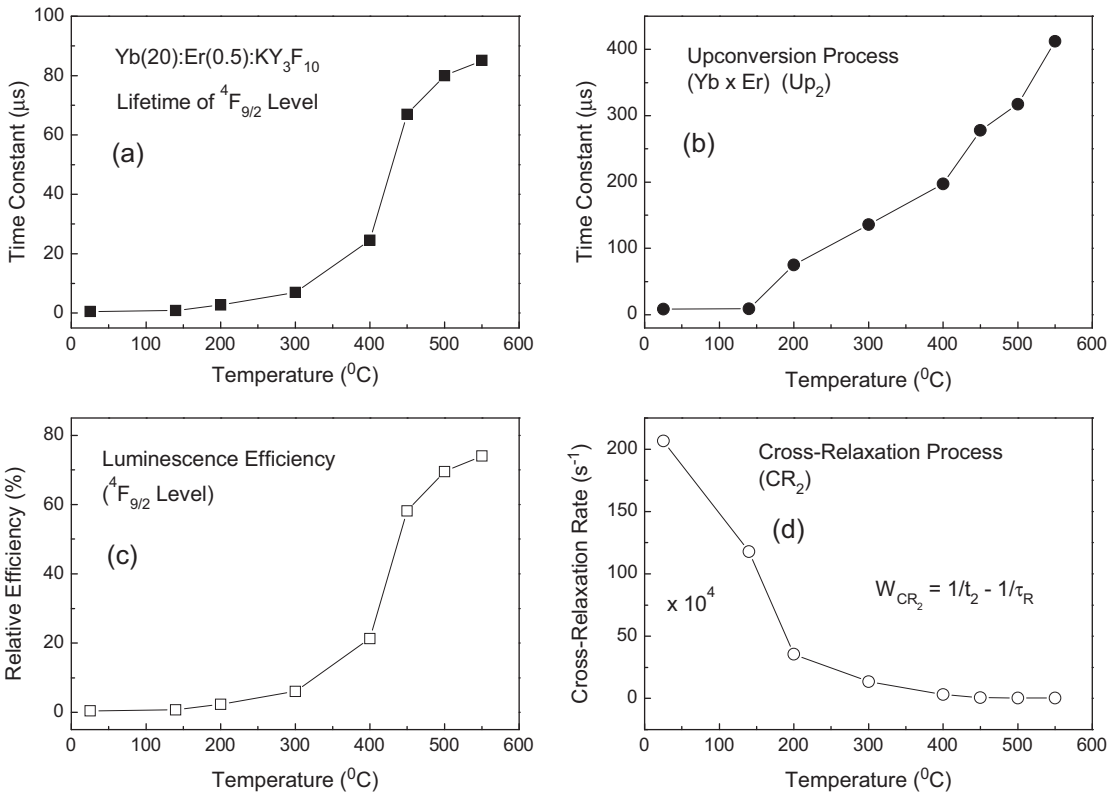

Fig. 11. Plot of measured lifetime of $^4F_{9/2}$ level of Er^{3+} (a), time constant of Yb^{3+} ($^2F_{5/2}$) × Er^{3+} ($^4I_{13/2}$) Up_2 process (b), luminescence efficiency ($^4F_{9/2}$) (c), and cross-relaxation rate (s^{-1}) calculated for $^4F_{9/2}$ level of Er^{3+} (d) as a function of the thermal treatment temperatures for Yb(20%):Er(0.5%):KY_3F_{10} synthesized nanopowder.

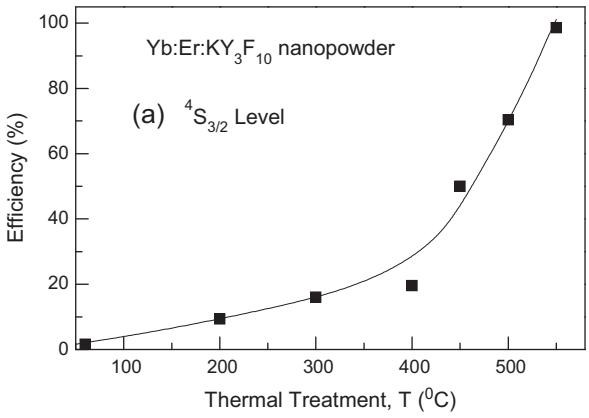

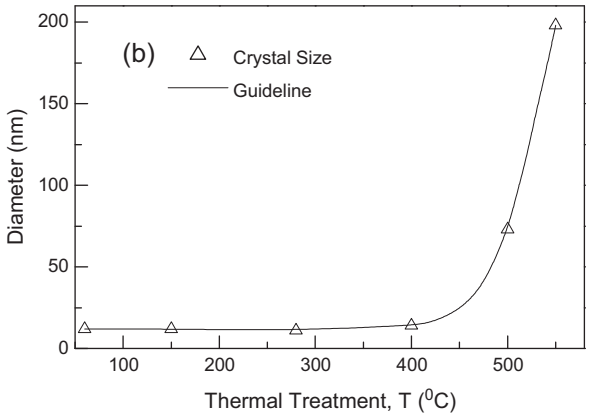

Fig. 12. Luminescence efficiency of $^4S_{3/2}$ level of Er^{3+} ion (a) and the mean diameter (or crystal size) (b) measured as a function of thermal treatment temperature of Yb (20%):Er(0.5%):KY_3F_{10} synthesized nanopowder.

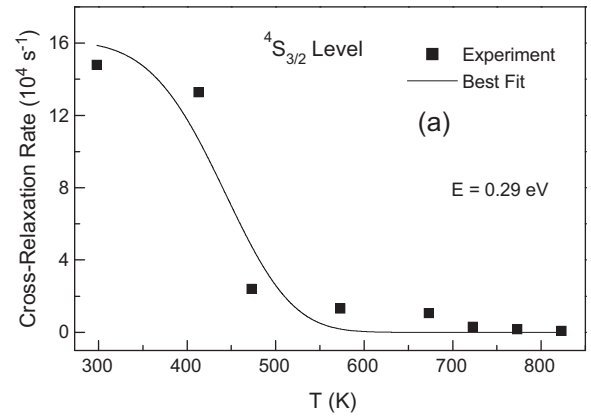

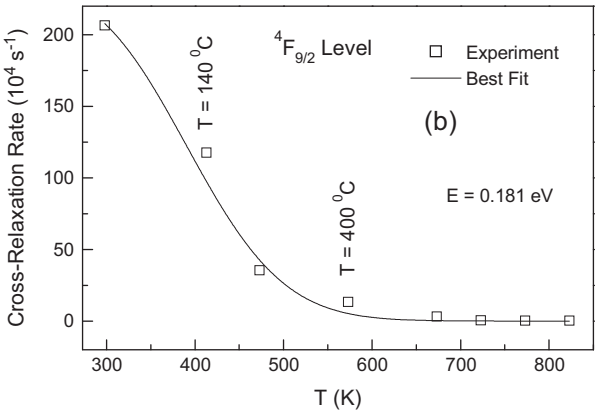

Fig. 13. Calculated rates (s^{-1}) for CR_1 and CR_2 processes due (Er × Er) cross-relaxations plotted as a function of the thermal treatment temperature (K) for the Yb(20%):Er(0.5%):KY_3F_{10} nanopowder. Best fittings to the experimental data were done using Eq. (6).

and 0.482 μs for $^4F_{9/2}$ levels (25 °C) drastically change to 413 μs ($^4S_{3/2}$) and 85 μs ($^4F_{9/2}$) after heat treatment to T = 550 °C.

The relative luminescence efficiencies of $^4S_{3/2}$ and $^4F_{9/2}$ levels were calculated using the relation $E_f = \frac{\tau_{nano}(T)}{\tau_{bulk}}$, where $\tau_{nano}(T)$ represents the measured lifetime of $^4S_{3/2}$ and $^4F_{9/2}$ levels of Er^{3+} for nanopowder and τ_{bulk} is the lifetime measured for the bulk crystal. Figs. 10(c) and 11(c) show that both $^4S_{3/2}$ and $^4F_{9/2}$ luminescence efficiencies strongly augment with the increasing of thermal treatment to T = 550 °C.

4. Discussion

The experimental observations obtained in this work from the luminescence kinetics measurements mentioned in the following give strong arguments to propose a physical description of the mechanisms that strong decreases the luminescence efficiencies of upconversion states of Er^{3+} in the synthesized (as grown) nanocrystals and how this effect can be minimized by thermal treatments in Yb:Er:KY_3F_{10}. (1) It is observed a competition between two upconversion processes, Up_1 and Up_2 in the synthesized (as grown) nanocrystal, besides the second (Up_2) be non-resonant with mismatch energy of 2000 cm^{-1}. In fact, a very short time constants were determined, i.e. t_{Up1} = 0.31 μs for Up_1 process and t_{Up2} = 8.2 μs (Up_2). Both time constants strongly increase with the thermal treatment temperature increasing to 550 °C, where the upconversion times approach to the upconversion times of the bulk crystal. (2) It is observed a very short lifetimes of $^4S_{3/2}$ and $^4F_{9/2}$ of Er^{3+} for the synthesized (as grown) nanocrystals due to the $Er^{3+}(^4S_{3/2}) \times Er^{3+}(^4I_{15/2})$ and $Er^{3+}(^4F_{9/2}) \times Er^{3+}(^4I_{15/2})$ cross-relaxations. Both lifetimes of $^4S_{3/2}$ and $^4F_{9/2}$ levels (Er^{3+}) strong increase with the increasing of thermal treatment (TT) to T = 550 °C, also approaching to the bulk crystal values.

The synthesized (as grown) nanopowder luminescence efficiencies are (i) 1.60% (as grown); 9.3% after TT = 200 °C; 20% (T = 400 °C) and 50% (T = 450 °C) for the $^4S_{3/2}$ level, and (ii) 0.4% (as grown); 2.4% after TT = 200 °C; 21% (T = 400 °C) and 58% (T = 450 °C) for the $^4F_{9/2}$ level. These effects on the lifetimes (t_1 or t_2) are due to the (Er × Er) cross-relaxations, CR_1 and CR_2 processes (Fig. 5), which decreases the $^4S_{3/2}$ and $^4F_{9/2}$ intrinsic lifetimes and consequently the luminescence efficiencies. Nevertheless, it is observed that the mean size of nanocrystals remains constant (8–12 nm) for thermal treatments with T < 450 °C, i. e., the crystallite size grows only for higher treatment temperatures (see Fig. 12). This result clearly shows that the mechanism responsible for the increasing of the luminescence efficiencies of $^4S_{3/2}$ and $^4F_{9/2}$ levels (Er^{3+}) is not dependent on the crystal size. However, this result indicates that the luminescence efficiencies of $^4S_{3/2}$ and $^4F_{9/2}$ levels enhance at expenses of the decreasing of the (Er × Er) cross-relaxations rates produced by a thermal activated Er^{3+} migration (or diffusion) during the nanocrystal thermal treatments with T > 100 °C.

The cross-relaxation rates of $^4S_{3/2}$ (W_{CR1}) and $^4F_{9/2}$ (W_{CR2}) excited states of Er^{3+} can be calculated using the equation $1/\tau_{nano} = 1/\tau_{bulk} + W_{CR}$, where τ_{nano} is the luminescence lifetime (experimental) given in Table 1. τ_{bulk} represents the total lifetime of $^4S_{3/2}$ and $^4F_{9/2}$ levels that includes the radiative decay, multi-phonon decay and the cross-relaxation rates measured for Er (0.5 mol.%) doped KY_3F_{10} bulk crystal, which are equal to 418 μs and 115 μs, respectively (see Table 2). Figs. 10(d) and 11(d) show the values of W_{CR} (s^{-1}) calculated for many temperatures of

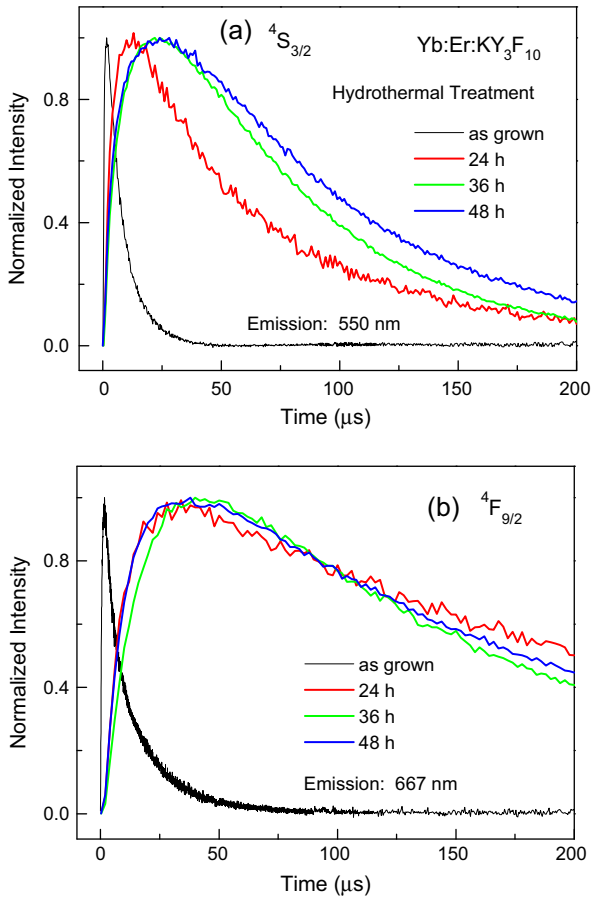

Fig. 14. Upconversion luminescence transient of $^4S_{3/2}$ (550 nm) (a) and $^4F_{9/2}$ (667 nm) (b) excited states of Er^{3+} measured for Yb(20):Er(0.5):KY_3F_{10} nanocrystals dispersed in water solution on a quartz cuvette under pulsed laser excitation at 972 nm (E = 8 mJ). Hydrothermal treatments were performed using the synthesized nanoparticles (not dried) dispersed in water solution put in a Teflon chamber closely tight inside of an stainless steel vessel kept at constant T = 200 °C for 24, 36, 48 or 60 h.

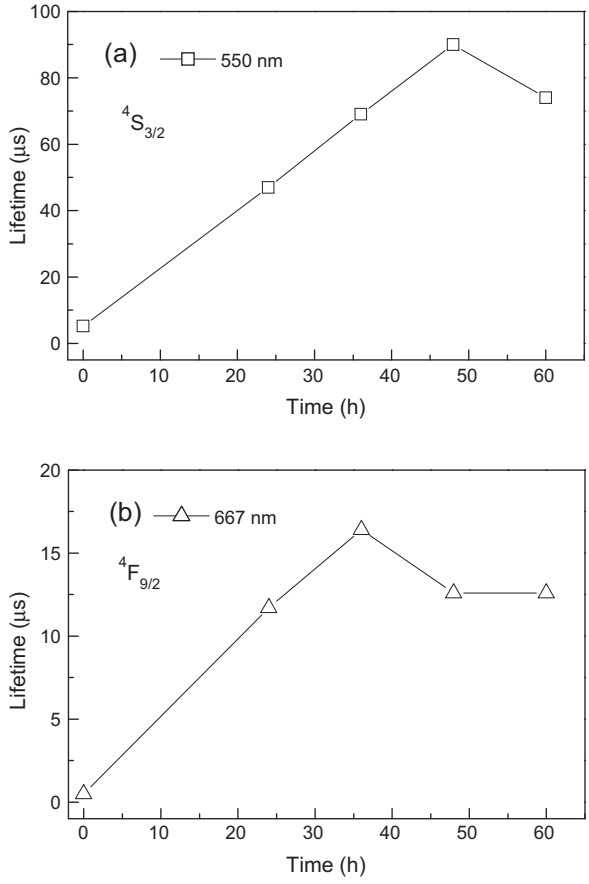

Fig. 15. Plot of the experimental lifetime values obtained for the $^4S_{3/2}$ and $^5F_{9/2}$ excited levels of Er^{3+} as a function of the hydrothermal treatment time (T = 200 °C).

thermal treatments for the $^4S_{3/2}$ and $^4F_{9/2}$ levels of Yb:Er:KY_3F_{10} nanopowder. In both cases, the cross-relaxation rate (s^{-1}) decreases as the heat treatment temperature increases, which infers that the Er^{3+} ion distribution changes towards be more homogeneous and random after T = 550 °C. We want to use the W_{CR2} (T) rate values in the Arrhenius model (first order process) to describe the cross-relaxation rate dependence on temperature exhibited in Fig. 11(d) as follows:

(1) The initial Er^{3+} concentration (or ion distribution) produced in the synthesized nanocrystal (T = 25 °C) depends exponentially on time duration (t) and temperature (T) of the thermal treatment as:

$$N(t) = N_0\, exp(-\alpha t); \quad \alpha = 1/\tau_{relax}; \quad \tau_{relax} = \tau_0\, exp(E/KT), \tag{4}$$

where N_0 is the initial concentration (Er), τ_{relax} is the relaxation time or the average time for the ion jump, E is the energy barrier (or activation energy) needed for the ion jump over the barrier, K is the Boltzmann constant, T is the temperature (Kelvin), and t is the time duration of thermal treatment at temperature T. Eq. (4) can be written also as

$$N(t,T) = N_0\, exp[-t/\tau_0\, exp(-E/KT)] \tag{5}$$

(2) Assuming that W_{CR} is dependent on the square of [Er^{3+}] concentration one can have the following function describing the (Er × Er) cross-relaxation rate as a function of the thermal treatment temperature (T) considering a thermal treatment time constant (or t = c) for each treatment for nanocrystals

$$W_{CR}(T) = W_0\, exp[-a\, exp(-b/T)], \tag{6}$$

where W_0, a and b are the fitting parameters. Fig. 13 shows the best fit curves to fit W_{CR1} (a) and W_{CR2} (b) versus thermal treatment temperature (T) by using Eq. (6) giving the following fitting parameters: (a) $W_0 = 1.61 \times 10^5 \pm (1.64 \times 10^4)\ s^{-1}$, $a = 2050$ and $b = 3512 \pm 122$ K ($R^2 = 0.938$); (b) $W_0 = 2.33 \times 10^6 \pm (1.42 \times 10^5)\ s^{-1}$, $a = 168$ and $b = 2172 \pm 356$ K ($R^2 = 0.996$). Using that $b = E/K$, where $K = 8.333 \times 10^{-5}$ eV/K we have the activation energies $E_1 = 0.28$ eV probed from the $^4S_{3/2}$ level decay and $E_2 = 0.18$ eV obtained using the $^4F_{9/2}$ level decay (see Fig. 13).

Table 4
Experimental values of the $^4S_{3/2}$ and $^4F_{9/2}$ excited states lifetimes and the luminescence efficiencies obtained after the hydrothermal treatment at T = 200 °C of Yb(20%):Er(0.5%):KY_3F_{10} nanocrystals dispersed in water solution for many treatment times.

Time (h)	$^4S_{3/2}$		$^4F_{9/2}$	
	t_1 (μs)	Ef (%)	t_2 (μs)	Ef (%)
Lifetime measured after hydrothermal treatments at T = 200 °C				
0	5.2	1.3	0.5	0.6
24	47	11	11.7	14
36	69	17	16.4	19
48	90	22	12.6	15
60	74	18	12.6	15

t_1 = 413 μs for $^4S_{3/2}$ and t_2 = 85 μs for $^4F_{9/2}$ level, respectively for the bulk crystal.

These measured activation energies of 0.18 and 0.28 eV gives a mean value of 0.23 eV what represents the thermal activation energy necessary for the Er^{3+} ion diffusion assisted by yttrium vacancy migration. This mean activation energy (0.23 eV) found for Er^{3+} to restore the intrinsic luminescence efficiency in thermally treated Yb:Er:KY_3F_{10} nanocrystals is consistent with the activation energy found in experiments of ionic diffusion of Ag^{++} ions in α-Cu_2S crystals (E = 0.198 eV), Li^{+} ions in α-AgI (0.198 eV), Au^{+} ions in KCl (1 eV) and Pb^{++} ions in PbI_2 crystals (1.29 eV) [29]. Recently we have measured an activation energy equal to 0.184 eV for Nd^{3+} ion diffusion in Nd:KY_3F_{10} nanocrystals using the experimental lifetime values of $^4F_{3/2}$ level as a function of the thermal treatment temperature and the Arrhenius model [30]. This fact indicates that the fast crystal growth imposed by the kinetic process and the growth tensions distribution tends to retard the impurity incorporation (RE^{3+}), wherefore generating the concentration gradient that affect the dynamic of the luminescence processes as upconversion and luminescence decay of a synthesized RE^{3+} - doped nanocrystal. By thermal treatments, this concentration effect will gradually diminish due to the RE^{3+} ions distribution that tends to be random as found in the bulk crystal (after heat treatment to 550 °C).

The proposed model explains the results of [31] that reports an improvement of the green emission efficiency of $^4S_{3/2}$ level of Er^{3+} in Yb:Er:$NaYF_4$ nanocrystals growth by co-precipitation in a solution kept at T = 320 °C for 1 h, where the RGR value increased ~15 times with respect to the synthesis done at T = 260 °C. At 320 °C, the ytterbium and erbium ions can diffuse thorough the crystal lattice improving a bit more the green luminescence efficiency due to the decrease of the (Er × Er) cross-relaxations, which is strong for the as grown $NaYF_4$ nanocrystal doped with [Er^{3+}] = 2 mol.%. According to our results the luminescence efficiency of green emission (Er^{3+}) increases by a factor of 10 for Yb:Er:KY_3F_{10} nanopowder after treatment to 300 °C. However, the luminescence efficiencies of $^4S_{3/2}$ and $^4F_{9/2}$ levels will be maximized only after treatment to T = 550 °C according to our results.

In the next we include our most recently results that shows the luminescence efficiency improvement of the $^4S_{3/2}$ (and $^4F_{9/2}$) level of Er^{3+} in Yb:Er:KY_3F_{10} synthesized nanocrystals done by hydrothermal treatment at T = 200 °C for many treatment times: 24, 36, 48 and 60 h. The upconversion luminescence transient effects are shown in Fig. 14. The luminescence transients were fit using Eq. (3) and the obtained lifetimes and efficiencies are listed in Table 4. Fig. 15 shows the lifetime increase of the $^4S_{3/2}$ (a) and $^4F_{9/2}$ (b) levels as a function of the duration time of the hydrothermal treatment. A strong luminescence efficiency increase is seen for the main fluorescent levels ($^4S_{3/2}$ and $^4F_{9/2}$) of Er^{3+}, besides the strong luminescence quenching observed to occur for the two lowest levels ($^4I_{13/2}$ and $^4I_{111/2}$) of Er^{3+} due to the energy transfer to OH^- ions mostly present in the nanoparticle surface.

5. Conclusions

One conclusion of this work is that the non-adiabatic and fast growth of nanocrystals introduces a non-random (Er^{3+} and Yb^{3+}) ions distribution that tends to increase the dopant concentration near the nanoparticle surface. The lifetime of $^4S_{3/2}$ state of Er^{3+} is a good reference parameter to indirectly evaluate how is the Er^{3+} ions distribution in the nanoparticle before and after thermal treatments. Its because this level has a strong concentration effects due to the (Er × Er) cross-relaxation that reduces the luminescence efficiency and has no effects due to the presence of OH^- ions bound in the nanoparticle surface. A similar lifetime effect was observed for the $^4S_{3/2}$ level of Er^{3+} using the as grown Yb:Er:KY_3F_{10} nanocrystals after hydrothermal treatment (HT) for 36 h and 48 h at T = 200 °C. In this case, the as synthesized nanocrystals were always kept dispersed in water solution before and after the hydrothermal treatment and during the luminescence measurements. After the hydrothermal treatment, the $^4S_{3/2}$ level lifetime increased from 5.2 μs (T = 25 °C) to 69 μs and 91 μs, respectively for 36 and 48 h.

Second conclusion is that the concentration gradient existing in the Yb:Er:KY_3F_{10} as grown nanocrystals allowed the Up_2 non-resonant process to compete with a resonant upconversion process (Up_1) exhibiting a very short upconversion time constant of 8.2 μs. However, decreasing the lifetimes of the $^4S_{3/2}$ and $^4F_{9/2}$ (Er^{3+}) excited states to 6.7 μs and 0.49 μs, respectively due to the strong (Er × Er) cross-relaxations. Nevertheless, the thermal treatment at T = 550 °C can restore the luminescence efficiencies of these levels to 99% for $^4S_{3/2}$ and 74% for $^4F_{9/2}$ excited levels relatively to the values found for the bulk crystal, however introducing a nanoparticle size augmentation (8.3 → 85 nm).

Acknowledgements

The authors thank financial support from FAPESP – Brazil (Grants Nos. 1995/4166-0 and 2000/10986-0) and CNPq – Brazil.

References

[1] H. Zheng, D. Gao, X. Zhang, E. He, J. Appl. Phys. 104 (1) (2008) 013506.
[2] Z. Chen, H. Chen, H. Hu, M. Yu, F. Li, Q. Zhang, Z. Zhou, T. Yi, C. Huang, J. Am. Chem. Soc. 130 (10) (2008) 3023.
[3] J. Zhou, F. Li, Chem. Soc. Ver. 41 (2012) 1323.
[4] J.C. Boyer, F. van Veggel, Nanoscale 2 (2010) 1417.
[5] Langping Tu, Xiaomin Liu, Fei Wu, Hong Zhang, Chem. Soc. Rev. 44 (2015) 1331.
[6] N.P. Barnes, IEEE J. Sel. Top. Quantum Electron. 13 (2007) 435.
[7] K. Friese, H. Kruger, V. Kahlenberg, T. Balic-Zunic, H. Emerich, J.-Y. Gesland, A. Grzechnik, J. Phys. – Condens. Matter 18 (2006) 2677.
[8] E. Boulma, M. Diaf, J.P. Jouart, M. Bouffard, J.L. Doualan, R. Moncorge, Opt. Mater. 30 (7) (2008) 1028.
[9] M. Ito, S. Hraiech, C. Goutaudier, K. Lebbou, G. Boulon, J. Crystal Growth 310 (2008) 140.
[10] K.J. Kim, A. Jouini, A. Yoshikawa, R. Simura, G. Boulon, T. Fukuda, J. Crystal Growth 299 (2007) 171.
[11] I.M. Ranieri, L.C. Courrol, A.F. Carvalho, L. Gomes, S.L. Baldochi, J. Mater. Sci. 42 (2007) 2309.
[12] H.M.S.M.D. Linhares, A.F.H. Librantz, L. Gomes, L.C. Courrol, S.L. Baldochi, I.M. Ranieri, J. Appl. Phys. 109 (2011) 08353.
[13] Tao Pang, Wanghe Cao, Mingming Xing, Xixian Luo, Xiaofei Yang, Opt. Mater. 33 (2011) 485.
[14] J.W. Mullin, Crystallization, fourth ed., Butterworth-Heinemann, Oxford, Boston, 2001.
[15] H.E. Buckley, Crystal Growth, Chapman and Hall, London, 1952.
[16] C. Sassoye, G. Patriarche, M. Mortier, Opt. Mater. 31 (8) (2009) 1177.
[17] A.C. Larson, R.B. Von Dreele, General Structure Analysis System (GSAS), Los Alamos National Laboratory Report LAUR 86, 2000.
[18] B.H. Toby, J. Appl. Crystallogr. 34 (2001) 210.
[19] Th.H. de Keijser, E.J. Mittemeijer, H.C.F. Rozendaal, J. Appl. Crystallogr. 16 (1983) 309.
[20] Bruker AXS, TOPAS V4.2, General Profile and Structure Analysis Software for Powder Diffraction Data Users's Manual, Bruker AXS, Karlsruhe, Germany, 2009.
[21] D. Balzar, N. Audebrand, M.R. Daymond, A. Fitch, A. Hewat, J.I. Langford, A. Le Bail, D. Louër, O. Masson, C.N. McCowan, N.C. Popa, P.W. Stephens, B.H. Toby, J. Appl. Crystallogr. 37 (2004) 911.
[22] H.M.S.M.D. Linhares, A.F.H. Librantz, L. Gomes, L.C. Courrol, S.L. Baldochi, I.M. Ranieri, J. Appl. Phys. 109 (2011) 083533.
[23] L.D. da Vila, L. Gomes, L.V.G. Tarelho, S.J.L. Ribeiro, Y. Messaddeq, J. Appl. Phys. 93 (2003) 3873.
[24] A.I. Burshtein, JETP Lett. 35 (1972) 885.
[25] A.F.H. Librantz, L. Gomes, J. Lumin. 129 (2009) 376.
[26] L. Gomes, M. Oermann, H. Ebendorff-Heidepriem, D. Ottaway, T. Monro, S.D. Jackson, J. Appl. Phys. 110 (2011) 083111.
[27] L. Gomes, S.D. Jackson, J. Opt. Soc. Am. B 30 (6) (2013) 1410.
[28] L. Gomes, J. Lousteau, D. Milanese, E. Mura, S.D. Jackson, J. Opt. Soc. Am. B 31 (3) (2014) 429.
[29] N.F. Mott, R.W. Gurney, Electronic Processes in Ionic Crystals, second ed., Dover Publications, Inc., New York, 1964.
[30] L. Gomes, H.M.S.M.D. Linhares, R.U. Ichikawa, L.G. Martinez, I.M. Ranieri, J. Lumin. 157 (2015) 285.
[31] Wenbin Niu, Suli Wu, Shufen Zhang, Jie Li, Lian Li, Dalton Trans. 40 (2011) 3305.
[32] S. Khiari, F. Bendjedaa, M. Diaf, Opt. Photon. J. 3 (2013) 13.